

# Mechanically transferred large-area Ga<sub>2</sub>O<sub>3</sub> passivates graphene and suppresses interfacial phonon scattering

Matthew Gebert,<sup>1,2</sup> Semonti Bhattacharyya,<sup>1,2,\*</sup> Christopher C Bounds,<sup>1</sup> Nitu Syed,<sup>3,4</sup> Torben Daeneke,<sup>4,5</sup> and Michael S. Fuhrer<sup>1,2,\*</sup>

<sup>1</sup>*School of Physics and Astronomy, Monash University, Victoria 3800, Australia*

<sup>2</sup>*ARC Centre of Excellence in Future Low-Energy Electronics Technologies, Monash University, Victoria 3800 Australia*

<sup>3</sup>*School of Physics, The University of Melbourne, Melbourne, Parkville VIC 3010, Australia*

<sup>4</sup>*School of Engineering, RMIT University, Melbourne, Victoria 3000, Australia*

<sup>5</sup>*ARC Centre of Excellence in Future Low-Energy Electronics Technologies, RMIT University, Melbourne, Australia 3000*

(Dated: June 7, 2022)

We demonstrate a large-area passivation layer for graphene by mechanical transfer of ultrathin amorphous Ga<sub>2</sub>O<sub>3</sub> synthesized on liquid Ga metal. A comparison of temperature-dependent electrical measurements of millimetre-scale passivated and bare graphene on SiO<sub>2</sub>/Si indicate that the passivated graphene maintains its high field effect mobility desirable for applications. Surprisingly, the temperature-dependent resistivity is reduced in passivated graphene over a range of temperatures below 220 K, due to the interplay of screening of the surface optical phonon modes of the SiO<sub>2</sub> by high-dielectric-constant Ga<sub>2</sub>O<sub>3</sub>, and the relatively high characteristic phonon frequencies of Ga<sub>2</sub>O<sub>3</sub>. Raman spectroscopy and electrical measurements indicate that Ga<sub>2</sub>O<sub>3</sub> passivation also protects graphene from further processing such as plasma-enhanced atomic layer deposition of Al<sub>2</sub>O<sub>3</sub>.

Keywords: “Chemical vapour deposition (CVD) Graphene”, “mm-scale oxide dielectric”, “passivation”, “remote interfacial polar phonon scattering”, “van der Waals heterostructure” “dielectric screening” “surface interface interaction”

Insulating layers are essential components of van der Waals heterostructures<sup>1</sup> isolating materials electronically, passivating them, and enabling electrostatic gating. High-quality hexagonal boron nitride (h-BN), hand-exfoliated from small single crystals, has been widely used as a wide bandgap insulator for vdW heterostructures, enabling exceptional device quality.<sup>2–5</sup> However, difficulties in producing large-area h-BN of similar quality<sup>6,7</sup> have so far precluded industrial-scale applications,<sup>8–10</sup> prompting a search for other suitable insulators to enable large-area vdW heterostructures.

In the case of encapsulating graphene, optimizing the material is highly complex; graphene’s electronic properties are largely

determined by the insulator’s properties, including charged impurity concentration,<sup>11</sup> dielectric constant,<sup>12</sup> and surface optical (SO) phonons which remotely scatter carriers in the graphene,<sup>13,14</sup> and trade-offs exist, e.g. insulators with intermediate dielectric constants may be optimal.<sup>15</sup>

Recently, the surface of liquid metals has been used to synthesize large-area atomically thin materials with facile mechanical transfer onto other substrates.<sup>7,16–19</sup> Indeed, Ga<sub>2</sub>O<sub>3</sub> has already been shown to be an excellent encapsulating layer for transition metal dichalcogenide crystals (TMDs),<sup>20</sup> preserving and even enhancing their optical properties.

Here we investigate liquid-metal synthesized Ga<sub>2</sub>O<sub>3</sub> as a large-area encapsulating layer for graphene with an intermediate relative static dielectric constant  $\kappa \sim 10$ .<sup>21</sup> We mechanically transfer large-area (millimeter-scale) Ga<sub>2</sub>O<sub>3</sub> onto one portion of a millimeter-scale graphene-on-SiO<sub>2</sub> device, allowing us to

---

\* Corresponding authors: semonti.bhattacharyya@monash.edu and michael.fuhrer@monash.edu

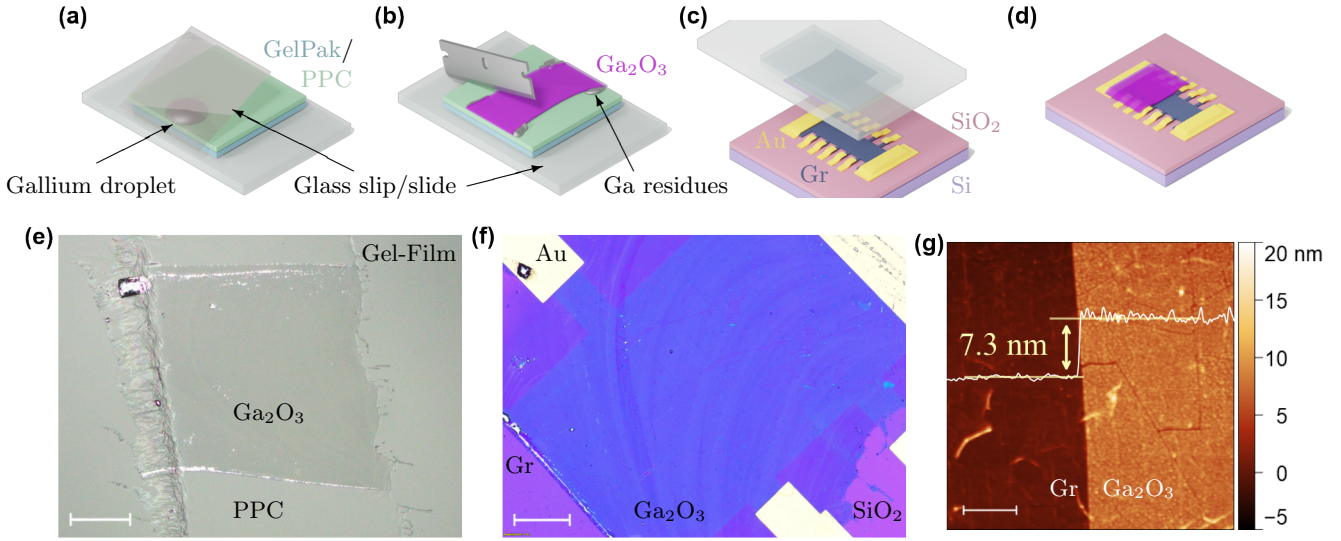


FIG. 1: Characterization of  $\text{Ga}_2\text{O}_3$  thin film transferred on Gr. Schematic representation of (a) Gallium metal positioned to be rolled across a PPC/Gel-Pak polymer stack using a cover slip, (b)  $\text{Ga}_2\text{O}_3$  after rolling with some Gallium metal residues, which can be cut away by a razor, (c) transfer of  $\text{Ga}_2\text{O}_3$  film onto Gr/ $\text{SiO}_2$ /Si device, and (d) device after removing polymer residues. (e) Optical darkfield micrograph of  $\text{Ga}_2\text{O}_3$  on PPC after cutting to size. The silver colored dots are liquid gallium droplets. The  $\text{Ga}_2\text{O}_3$  sheet at the centre is bordered by liquid gallium. The scale bar is  $200 \mu\text{m}$ . (f) Brightfield optical micrograph of  $\text{Ga}_2\text{O}_3$  (deep blue sheet on the device) transferred on Gr-device. The scale bar is  $50 \mu\text{m}$ . (g) Topographic image of  $\text{Ga}_2\text{O}_3$ -on-Gr sheet obtained by intermittent contact atomic force microscopy (AFM). The left side of the image shows bare Gr, and right side of the image shows  $\text{Ga}_2\text{O}_3$ -covered Gr. Mean height difference is  $7.3 \text{ nm}$  as shown in the overlaid line profile, and the scalebar is  $2 \mu\text{m}$ .

compare the electronic transport properties of bare and  $\text{Ga}_2\text{O}_3$ -encapsulated portions of the same device. We find that coating graphene with  $\text{Ga}_2\text{O}_3$  preserves the charge carrier mobility close to  $3,000 \text{ cm}^2\text{V}^{-1}\text{s}^{-1}$ . Surprisingly, we observe a reduction in temperature-dependent resistivity at temperatures below  $220 \text{ K}$  in the graphene encapsulated by the  $\text{Ga}_2\text{O}_3$  dielectric, explained by the interplay of screening of the SO phonon modes of the  $\text{SiO}_2$  by high-dielectric-constant  $\text{Ga}_2\text{O}_3$ , and the relatively high characteristic phonon frequencies of  $\text{Ga}_2\text{O}_3$  itself. We further show that  $\text{Ga}_2\text{O}_3$  is useful as a passivation layer, protecting against damage from deposition of  $\text{Al}_2\text{O}_3$  via plasma enhanced ALD.

Devices were fabricated (see Section S1 and S2, Supporting Information) using a

commercial (Graphene Supermarket) CVD-grown monolayer graphene/monolayer h-BN film (henceforth referred to as “Gr”) already transferred onto  $285 \text{ nm}$   $\text{SiO}_2$ /Si (p-doped) substrate that functions as a global back-gate dielectric and electrode. The Gr was then etched into a Hall bar geometry  $0.4 \text{ mm}$  wide and  $1.2 \text{ mm}$  long, with multiple voltage electrodes spaced by  $0.25 \text{ mm}$ , and contacted by Ti/Au electrodes fabricated using conventional photolithography. Next, mm-scale ultrathin  $\text{Ga}_2\text{O}_3$  was prepared on a PPC film on a PDMS stamp (Gel-film, Gelpak) through a liquid metal “squeeze-printing”<sup>19</sup> technique. Finally,  $\text{Ga}_2\text{O}_3$  was deterministically transferred onto half of the Gr device.<sup>20</sup> We compare the experimental signatures of ‘bare’ and ‘ $\text{Ga}_2\text{O}_3$ -covered’ parts of graphene in the same

Hall bar device to understand the effect of  $\text{Ga}_2\text{O}_3$ .

Figure 1 illustrates the steps in the construction of the  $\text{Ga}_2\text{O}_3$ -on-Gr device. The process of transferring ultrathin  $\text{Ga}_2\text{O}_3$  films on such Gr-devices are schematically represented in Fig. 1a-d). First, a mm-scale ultrathin  $\text{Ga}_2\text{O}_3$  film was prepared on a PPC film mounted on a PDMS stamp through a liquid metal printing technique known as “squeeze-printing”<sup>19</sup> (Fig. 1a). This film was then cut into appropriate size to cover half of the Gr-device as well as to get rid of additional Ga-particles (Fig. 1b), and was finally deterministically transferred onto half of the Gr Hall bar device using a home-made van der Waals stacking set up<sup>20</sup> (Fig. 1c and d).

Figure 1e) shows a dark-field image of a squeeze-printed  $\text{Ga}_2\text{O}_3$  film on PPC/PDMS assembly. This film was trimmed to  $0.7 \text{ mm} \times 0.65 \text{ mm}$  to match the Gr-device. The dark-field image highlights the Ga-metal residue, left from the squeeze-printing process, which is negligible in the interior area of the film, and mostly appears at the boundary. Figure 1f) shows a bright-field optical image of the  $\text{Ga}_2\text{O}_3$  film transferred on the Gr-device. The optical contrast of the amorphous  $\text{Ga}_2\text{O}_3$  film is largely uniform, though slight variations are visible, indicating similar thickness across the thin film (Section S9, Supporting Information). Figure 1g) shows an atomic force micrograph of both  $\text{Ga}_2\text{O}_3$ -covered (right-half) and bare side (left-half) of a Gr-device. The AFM line profile (overlaid) yields a step height of 7.3 nm for  $\text{Ga}_2\text{O}_3$ , similar to AFM measurements performed on similar devices (Section S9, Supporting Information), and consistent with thicknesses reported by Wurdack *et al.*<sup>20</sup>

Figure 2 compares the gate-voltage and temperature dependent electrical transport properties of the bare and  $\text{Ga}_2\text{O}_3$ -covered Gr-devices. The 3D schematic of the device and top-view micrograph are shown in Figure 2a) and b) respectively. Figure 2b) shows that the transferred  $\text{Ga}_2\text{O}_3$  film covers half of the Gr-device. The orientation of the  $\text{Ga}_2\text{O}_3$  film has been carefully controlled so that the Ga-metal particles at the boundary do not affect the electrical transport characteristics between the voltage probes.

Figure 2c) shows the gate voltage ( $V_g$ )-dependence of the longitudinal conductivity  $\sigma$  measured at temperature  $T = 100 \text{ K}$  for both bare and  $\text{Ga}_2\text{O}_3$  covered Gr. The gate voltage  $V_g$  is offset by the gate voltage of minimum conductivity ( $V_{g,min} = -1.2 \text{ V}$  and  $-26.2 \text{ V}$  respectively for the bare and  $\text{Ga}_2\text{O}_3$ -covered sides) to facilitate comparison between the two sides of the device. The comparison of the two parts of the sample shows three notable differences, with the  $\text{Ga}_2\text{O}_3$ -covered part showing (i) slightly enhanced conductivity at high  $V_g$ , (ii) increased magnitude of minimum conductivity  $\sigma_{min}$ , and (iii) a broader minimum-conductivity plateau.

In order to highlight the first of these features we plot the field effect mobility ( $\mu_{FE} = \frac{1}{c_g} \frac{\partial \sigma}{\partial V_g}$ ;  $c_g =$  Capacitance of the  $\text{SiO}_2$  back gate) obtained from  $\sigma(V_g)$  data (Figure 2d). The peak electron mobility is slightly improved in the  $\text{Ga}_2\text{O}_3$ -covered graphene ( $\mu = 2900 \text{ cm}^2\text{V}^{-1}\text{s}^{-1}$ ) relative to bare graphene ( $\mu = 2800 \text{ cm}^2\text{V}^{-1}\text{s}^{-1}$ ). The highest observed hole mobility in  $\text{Ga}_2\text{O}_3$ -covered Gr ( $\mu = 2200 \text{ cm}^2\text{V}^{-1}\text{s}^{-1}$ ) is lower than in bare Gr ( $\mu = 3000 \text{ cm}^2\text{V}^{-1}\text{s}^{-1}$ ) but might not be a global maximum, as it is at the edge of the  $V_g$  measurement window.  $\mu_{FE}$  is observed to be mostly unchanged by the addition of  $\text{Ga}_2\text{O}_3$ , if not a little increased at high positive  $V_g$ .

The slight enhancement of mobility after deposition of  $\text{Ga}_2\text{O}_3$  is remarkable because previous experiments found that deposition of oxide usually degrades the mobility of graphene<sup>22</sup> due to introduction of disorder. In contrast, screening by a clean dielectric can reduce charged impurity scattering.<sup>12,23</sup> To infer the impurity concentration in  $\text{SiO}_2/\text{Gr}/\text{Ga}_2\text{O}_3$  with RPA-Boltzmann theory<sup>24</sup> we use  $\kappa = 10$  for the amorphous  $\text{Ga}_2\text{O}_3$ ,<sup>21</sup> and  $\mu = 2900 \text{ cm}^2\text{V}^{-1}\text{s}^{-1}$  and calculate an impurity concentration of  $n_{imp,\text{Ga}_2\text{O}_3} = 3.8 \times 10^{12} \text{ cm}^{-2}$  (Section S6.A in the Supporting Information), roughly twice the impurity concentration inferred for our bare graphene on  $\text{SiO}_2$  ( $n_{imp,bare} = 1.8 \times 10^{12} \text{ cm}^{-2}$ ). This indicates that our liquid-metal synthesized and mechanically transferred  $\text{Ga}_2\text{O}_3$  layer has low charged impurity concentration, comparable to thermally grown  $\text{SiO}_2$ .

According to the RPA-Boltzmann theory,

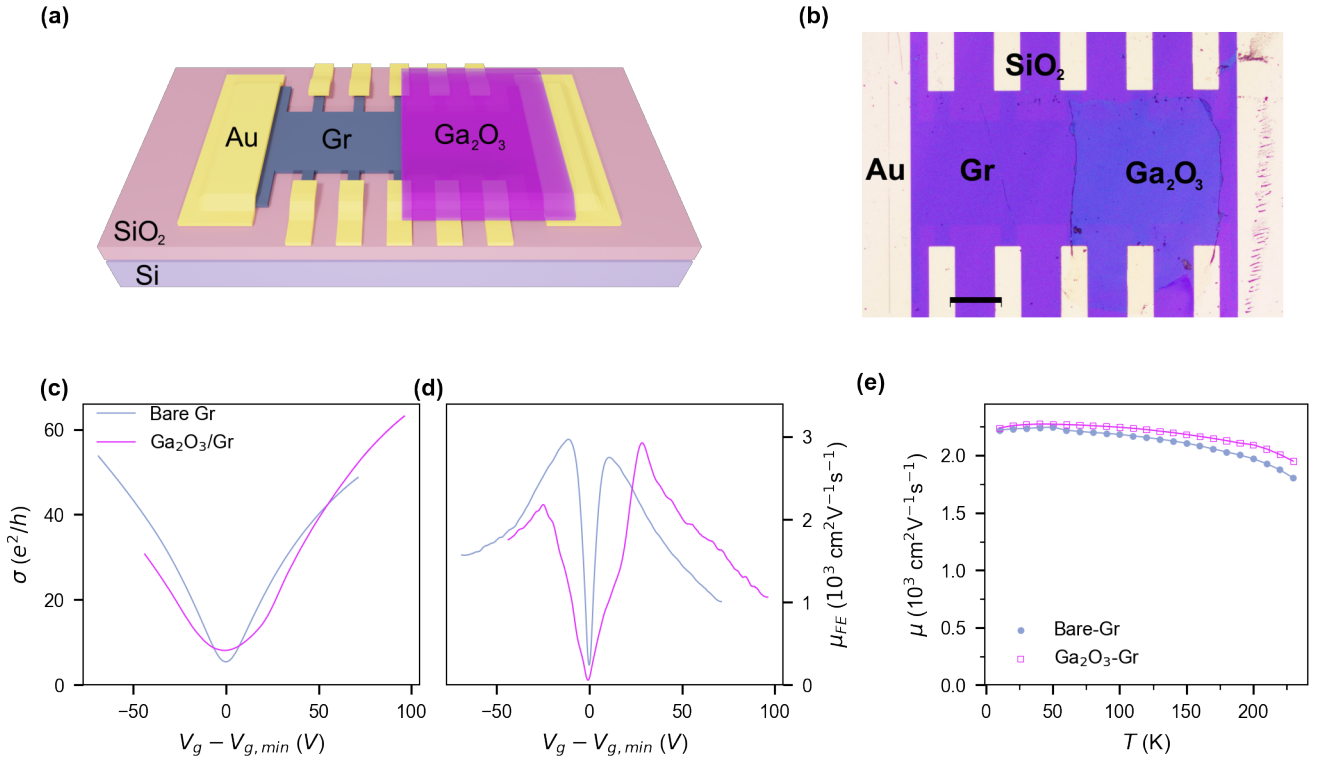


FIG. 2: Gate voltage and temperature dependent electrical transport measurements of  $\text{Ga}_2\text{O}_3$ -covered and bare Gr field effect devices. **(a)** Schematic illustration and **(b)** optical microscope image of a Gr-device after  $\text{Ga}_2\text{O}_3$  transfer. The scale bar is  $200 \mu\text{m}$ . **(c)** Longitudinal conductivity  $\sigma$  and **(d)** field-effect mobility  $\mu_{\text{FE}}$  as a function of gate voltage  $V_g$  offset by gate voltage at minimum conductivity  $V_{g,\text{min}}$ , for both bare Gr and  $\text{Ga}_2\text{O}_3$ -covered Gr at 100 K. **(e)** Temperature ( $T$ )-dependent mobility ( $\mu$ ) calculated at charge carrier density  $n = 5 \times 10^{12} \text{ cm}^{-2}$ .

the increased  $n_{\text{imp}}$  should also lead to a very weak reduction of  $\sigma_{\text{min}}$ <sup>24</sup> and a narrowing of the minimum conductivity plateau in the  $\text{Ga}_2\text{O}_3$ -covered graphene (Section S6.B in the Supporting Information), in contrast to our observation (Figure 2c). The increased  $\sigma_{\text{min}}$ , as well as broadening of the minimum conductivity plateau likely instead reflect additional macroscopic inhomogeneity of the sample<sup>25</sup> induced by the  $\text{Ga}_2\text{O}_3$ .

In order to further explore the modification of electrical transport in  $\text{Ga}_2\text{O}_3$ -covered graphene we plotted  $\mu = \frac{\sigma}{ne}$  calculated at  $n = 5 \times 10^{12} \text{ cm}^{-2}$  for both bare and  $\text{Ga}_2\text{O}_3$ -covered graphene (Figure 2e). We observe a

gradual reduction in mobility with increasing temperature between 60 K to  $\approx 220$  K in both. The overall decline of mobility indicates a temperature-dependent resistivity contribution, which surprisingly appears larger in bare compared to  $\text{Ga}_2\text{O}_3$ -covered graphene, in contrast to previous experiments where addition of an oxide layer on graphene increased the temperature-dependent resistivity.<sup>26</sup>

We expect that dielectric layers affect the temperature dependent mobility of graphene through scattering of charge carriers by SO phonons. This process, also known as remote optical phonon (ROP) scattering, is expected to contribute a resistivity proportional to a

Bose-Einstein distribution.<sup>14</sup>

$$\rho_{ROP}(V_g, T) = V_g^{-\alpha} \sum_i^M \frac{\beta_i}{e^{\hbar\omega_i/k_B T} - 1} \quad (1)$$

Here the  $i^{\text{th}}$  SO mode is described by the SO phonon energy  $\hbar\omega_i$  (meV) and respective coupling strength  $\beta_i$  ( $V_g^\alpha$ ). Empirically the dependence on gate voltage is found to follow a power law with  $\alpha \approx 1$ .

To examine the differences in ROP scattering for bare and  $\text{Ga}_2\text{O}_3$ -covered graphene, we extracted  $\rho_{ROP}(V_g, T)$  from  $\rho(V_g, T)$  (see Section S10, Supporting Information for details). Briefly, we perform a global fit of  $\rho(V_g, T)$  at different  $V_g$  at  $70 \text{ K} \leq T \leq 100 \text{ K}$  to determine the acoustic phonon scattering contribution  $\rho_{LA}(T)$  which is linear in temperature and independent of  $V_g$ , and the impurity contribution  $\rho_{imp}(V_g, T = 0 \text{ K})$  which depends on  $V_g$  but not temperature. Subtracting these two quantities from  $\rho(V_g, T)$  allows us to extract  $\rho_{ROP}(V_g, T)$ .

Figure 3a) shows the contribution of ROP scattering  $\rho_{ROP}(V_g, T)$  to resistivity as a function of temperature, for various positive gate voltages (offset from the minimum  $V_{g,min}$ ).  $\rho_{ROP}(V_g, T)$  increases super-linearly in temperature, with larger magnitude at smaller  $V_g - V_{g,min}$ . Remarkably, in the temperature range  $70 - 220 \text{ K}$ ,  $\rho_{ROP}$  is lower in the  $\text{Ga}_2\text{O}_3$ -covered Gr compared to bare Gr for all values of  $V_g - V_{g,min}$ . The dashed lines in Figure 3a) are global fits of the data to Eq. (1) for a single phonon mode ( $M = 1$ ) for bare (dashed) and  $\text{Ga}_2\text{O}_3$ -covered (dot-dash) graphene.

The results of the fits in Figure 3a) are summarized in Table I. We determine the SO mode energy,  $\hbar\omega_0$ , to be larger in  $\text{Ga}_2\text{O}_3$ -covered graphene (92.8 meV) compared to bare graphene on  $\text{SiO}_2$  (69.5 meV). The observation of slightly higher  $\hbar\omega_0$  compared to the expected lowest phonon mode for  $\text{SiO}_2$  (61 meV) was also observed by Chen *et al.*,<sup>14</sup> and likely due to additional contribution of the higher-energy  $\text{SiO}_2$  mode. The power-law exponent  $\alpha$  is similar for bare and  $\text{Ga}_2\text{O}_3$ -covered graphene, and close to that of previous literature.<sup>14,26</sup> The coupling strength  $\beta$  is found to be  $6.0$  ( $h/e^2$ ) for bare graphene, which is roughly double the value of  $3.26$

( $h/e^2$ ) found by Chen *et al.*<sup>14</sup> Due to the different values of  $\alpha$  for  $\text{Ga}_2\text{O}_3$ -covered graphene, it is difficult to directly compare the coupling  $\beta$  which has different dimensions and consequently has a different magnitude to that for bare graphene.

Our observations (Table I) indicate that the smaller magnitude of  $\rho_{ROP}(V_g, T)$  at low temperatures ( $T \lesssim 220 \text{ K}$ ) for  $\text{Ga}_2\text{O}_3$ -covered graphene is due to a higher effective phonon energy, resulting in a lower  $\rho_{ROP}(V_g, T)$  at low temperatures due to lower phonon population, and eventually crossing over to higher  $\rho_{ROP}(V_g, T)$  at high  $T$  due to stronger coupling. To better understand the lower  $\rho_{ROP}$  contribution in  $\text{Ga}_2\text{O}_3$ -covered graphene, we develop a simple analytical model of the  $\text{SiO}_2/\text{graphene}/\text{Ga}_2\text{O}_3$  heterostructure, following the methodology used in semiconductor inversion layers<sup>27</sup> and graphene systems.<sup>13,26</sup> The details of the model are described in the Section S8 Supporting Information.

The resultant phonon frequencies and coupling constants of both bare and  $\text{Ga}_2\text{O}_3$ -covered graphene is schematically represented in Fig. 3b) (see Table S2, S3-S6, Supporting Information for more details). We find that the graphene/ $\text{SiO}_2$  structure has two SO modes i.e.,  $\hbar\omega_1 = 61 \text{ meV}$  and  $\hbar\omega_2 = 149 \text{ meV}$ .  $\text{Ga}_2\text{O}_3/\text{graphene}/\text{SiO}_2$  structure has three SO modes, with energies and coupling strengths shown in Fig. 3b). Here  $\hbar\omega'_1 = 56 \text{ meV}$ ,  $\hbar\omega'_2 = 147 \text{ meV}$  are the perturbed  $\text{SiO}_2$  modes, while  $\hbar\omega'_3 = 95 \text{ meV}$  originates in  $\text{Ga}_2\text{O}_3$ . While all these modes are thermally activated, the  $\text{Ga}_2\text{O}_3$  mode couples particularly strongly, also reflected in the high disparity between  $\epsilon_{\text{Ga}_2\text{O}_3}^0$  and  $\epsilon_{\text{Ga}_2\text{O}_3}^\infty$  (Table S2 and Section S8, Supporting Information). At the same time however, the large  $\epsilon_{\text{Ga}_2\text{O}_3}^\infty$  screens the ROP scattering from  $\text{SiO}_2$  modes. Hence we expect the  $\omega'_3$  mode to dominate the temperature-dependent resistivity. Importantly, the energy corresponding to the  $\omega'_3$  mode matches well with the  $\hbar\omega_0$  value obtained from fitting our experimental data (Fig. 3a) and Table I.

Figure 3c) shows the analytically obtained  $\rho_{ROP}(T)$  for the  $\text{Ga}_2\text{O}_3/\text{graphene}/\text{SiO}_2$  structure and bare graphene/ $\text{SiO}_2$  calculated using Eq. (1), using the SO modes as shown in Fig. 3c) (also given in Table S3 and

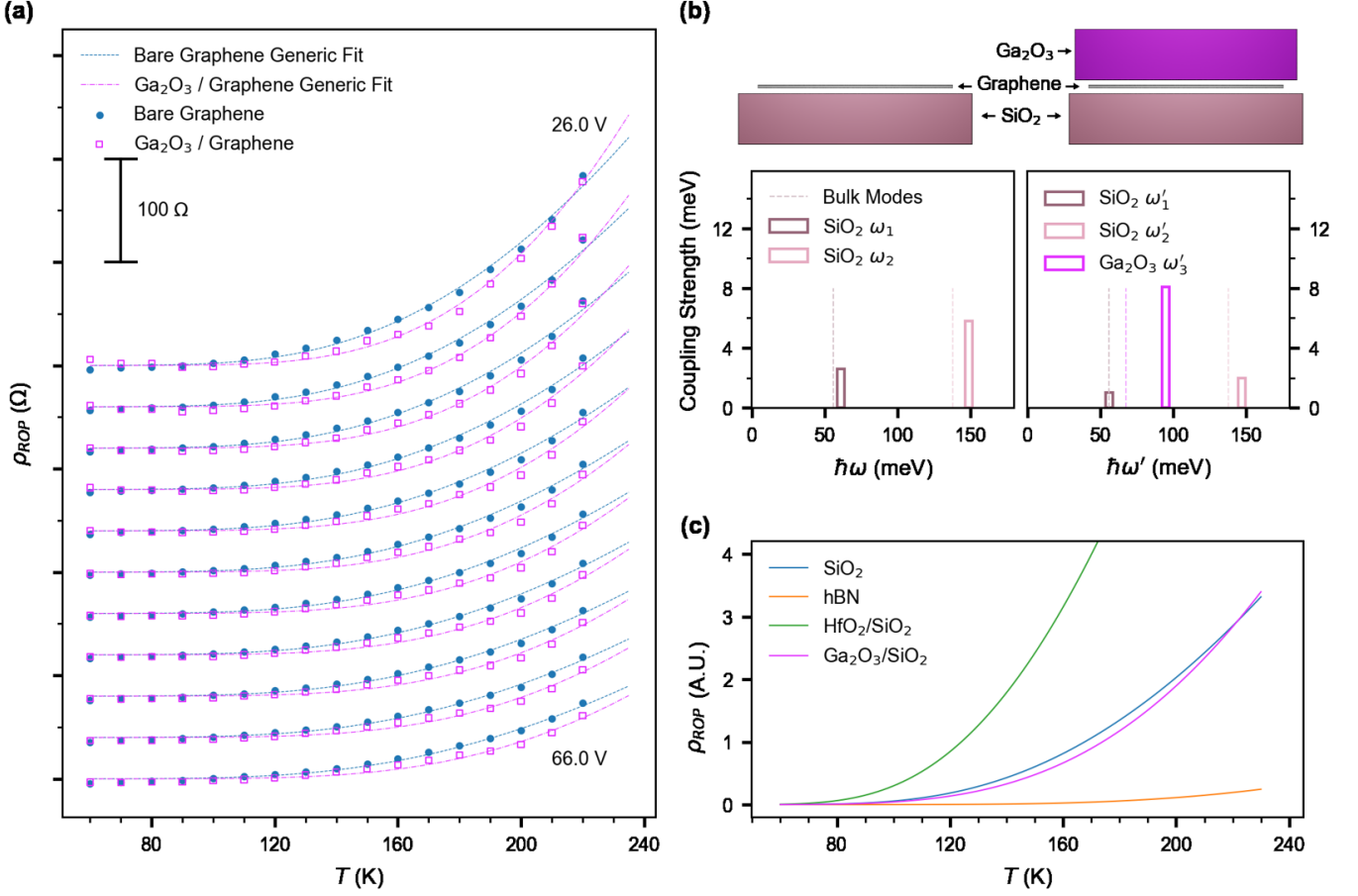


FIG. 3: **Remote optical phonon (ROP) Scattering** (a) ROP contributions to resistivity ( $\rho_{ROP}$ ) extracted from the temperature ( $T$ )-dependence of resistivity ( $\rho$ ) in bare (filled) and  $\text{Ga}_2\text{O}_3$ -covered (hollow) graphene. Fits using Eq. (1) are plotted with dashed line for bare and dot-dashed line  $\text{Ga}_2\text{O}_3$ -covered Gr. Each gate voltage, from 26 V through 66 V via 4 V steps,  $\rho_{ROP}$  is offset by 40  $\Omega$ . (b) Computed frequency and coupling strength of SO phonons in bare and  $\text{Ga}_2\text{O}_3$ -covered Gr. Dashed lines indicate the corresponding bulk mode phonon frequency. (c) Modelled ROP scattering contribution to the resistivity ( $\rho_{ROP}$ ) in graphene for different dielectric systems.

Table S6, Supporting Information). Also shown for comparison are graphene/h-BN, and  $\text{HfO}_2/\text{graphene}/\text{SiO}_2$  (Table S4, S5, Supporting Information). We see that  $\rho_{ROP}(T)$  in  $\text{Ga}_2\text{O}_3/\text{graphene}/\text{SiO}_2$  is lower than for bare graphene/ $\text{SiO}_2$  at temperatures below approximately 220 K. Because ROP is thermally activated, at low temperatures the  $\text{SiO}_2$  mode ( $\omega_1$ ) will dominate  $\rho_{ROP}$  for bare graphene/ $\text{SiO}_2$ , while for the  $\text{Ga}_2\text{O}_3/\text{graphene}/\text{SiO}_2$  structure,

the  $\text{Ga}_2\text{O}_3$  effectively screens these  $\text{SiO}_2$  contributions. At higher  $T$ , the higher mode energy ( $\omega'_3 > \omega'_1$ )  $\text{Ga}_2\text{O}_3$  ROP scattering becomes active and quickly begins to dominate due to the higher coupling. Our observation that addition of  $\text{Ga}_2\text{O}_3$  to graphene/ $\text{SiO}_2$  can lower the overall interfacial phonon scattering may inspire the design of other heterostructures to further reduce scattering phenomena of charge carriers in graphene, perhaps yield-

TABLE I: Parameters for fits of data in Figure 3 for bare and Ga<sub>2</sub>O<sub>3</sub>-covered graphene to Equation (1)

	$\alpha$	$\beta$ (V <sup>-<math>\alpha</math></sup> h/e <sup>2</sup> )	$\hbar\omega_0$ (meV)
Bare	0.97 ± 0.03	6.0 ± 1.1	69.5 ± 1.3
Ga <sub>2</sub> O <sub>3</sub>	1.18 ± 0.03	43.1 ± 6.7	92.8 ± 2.6

ing a more significant improvement at or above room temperature.

In our model, we have ignored the effect of the monolayer h-BN in between graphene and SiO<sub>2</sub>. The model agrees well with experiment and past literature,<sup>11,26</sup> suggesting that the surface modes of h-BN/SiO<sub>2</sub> are comparable to that of bare SiO<sub>2</sub>. This may be explained by the similar dielectric constants of the SiO<sub>2</sub> and h-BN resulting in similar SO properties for the monolayer h-BN/SiO<sub>2</sub> composite to bare SiO<sub>2</sub>. Our model on SiO<sub>2</sub>/graphene/HfO<sub>2</sub> device matches with previous results as expected.<sup>26</sup>

Having demonstrated that Ga<sub>2</sub>O<sub>3</sub> does not enhance impurity scattering in graphene and even reduces the impact of phonon scattering in a certain temperature range, we now investigate whether Ga<sub>2</sub>O<sub>3</sub> is effective in protecting graphene from further processing. Methods of growing large-area dielectric films, such as CVD, atomic layer deposition (ALD), sputtering, e-beam evaporation have proven to be damaging for graphene, leading to enhancement of impurity scattering, and consequently degradation of mobility.<sup>26,28-32</sup>

Our gentle transfer technique for thin Ga<sub>2</sub>O<sub>3</sub> avoids such damaging processes, as demonstrated in Figure 2. We further demonstrate the protective nature of Ga<sub>2</sub>O<sub>3</sub> by using plasma-enhanced ALD to grow a 5.5 nm layer of Al<sub>2</sub>O<sub>3</sub> over the entire sample, following the method of Tang *et al.*<sup>29</sup> (see Section S3, Supporting Information for further details), in order to replicate conditions that normally might damage graphene. The ALD chamber temperature is modified to 150° C, to avoid possible change of morphology of amorphous Ga<sub>2</sub>O<sub>3</sub> by thermal annealing.<sup>20</sup>

Figure 4 compares the effect of Al<sub>2</sub>O<sub>3</sub> deposition on the bare and the Ga<sub>2</sub>O<sub>3</sub>-covered side of the Gr device. Figure 4a) and b) show Raman spectra on bare and Ga<sub>2</sub>O<sub>3</sub>-covered

sides respectively before and after ALD deposition. Both areas of the device show monolayer graphene G & 2D Raman peaks at 1591 cm<sup>-1</sup> and 2709 cm<sup>-1</sup>, with expected ratio ~2. Before ALD deposition the graphene spectra on both sides are nearly identical, confirming that Ga<sub>2</sub>O<sub>3</sub>-transfer process does not lead to any structural disorder in graphene. However, there is a stark difference between the Raman spectra on both sides of the devices after ALD processing, where the bare graphene area shows a fully formed D-peak (1357 cm<sup>-1</sup>), which is nearly absent in pre-processed graphene, and remains unchanged in the Ga<sub>2</sub>O<sub>3</sub>-covered graphene even after processing. The D peak is activated by point disorder, and indicates deposition-induced damage in bare graphene which is not present in Ga<sub>2</sub>O<sub>3</sub>-covered graphene. This clearly indicates that Ga<sub>2</sub>O<sub>3</sub> transfer has no adverse effect on graphene, and also acts as an encapsulating layer to protect graphene against further damage during subsequent deposition processes.

This is further supported through electrical transport data obtained on both sides of an identically prepared device before and after Al<sub>2</sub>O<sub>3</sub> deposition (Fig. 4c-f). Figure 4c,d) and Figure 4e,f) show the relative change in  $\sigma$  and  $\mu_{FE}$  respectively before and after ALD, both on bare and Ga<sub>2</sub>O<sub>3</sub>-covered graphene. After ALD processing, there is a global decrease in  $\sigma$  and  $\mu_{FE}$  for bare graphene, and peak  $\mu$  drops by  $\approx 30\%$ , compared to  $< 15\%$  in Ga<sub>2</sub>O<sub>3</sub>-covered graphene. At higher gate voltages ( $V_g - V_{g,min} > 50$  V) the transport in processed Ga<sub>2</sub>O<sub>3</sub>-covered graphene shows similar performance to prior to ALD, with higher  $\mu_{FE}$  values, and similar  $\sigma$  at  $\approx 100$  V. The broadening (and slight reduction) of the  $\mu_{FE}$  peak in the Ga<sub>2</sub>O<sub>3</sub>-covered side (Fig. 4f) appears to have been caused by further enhancement of the inhomogeneity already present in the system, as the higher mobility at high car-



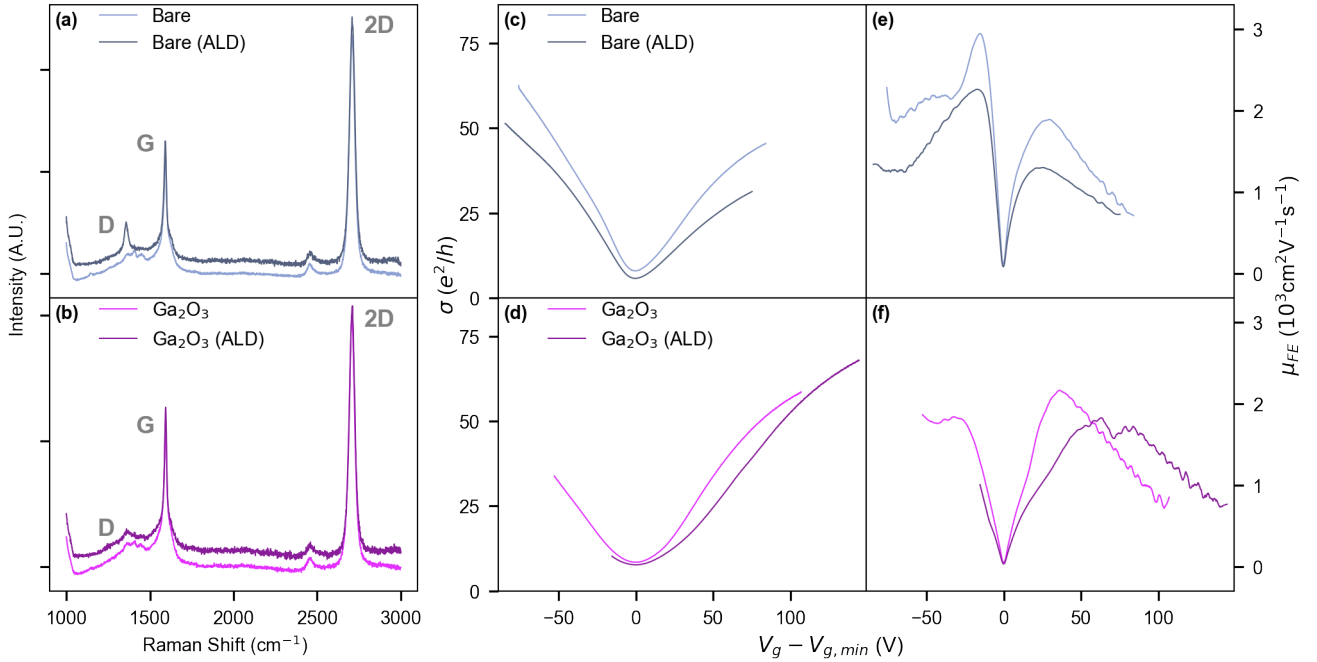


FIG. 4:  $\text{Ga}_2\text{O}_3$  as a protective layer on graphene against plasma-enhanced atomic layer deposition (ALD) of  $\text{Al}_2\text{O}_3$ . Raman spectroscopy with D, G and 2D peaks indicated for (a) bare graphene and (b)  $\text{Ga}_2\text{O}_3$ -covered graphene. Gate-dependence of conductivity ( $\sigma$ ) and mobility ( $\mu_{FE}$ ) respectively for (c, e) bare Gr and (d, f)  $\text{Ga}_2\text{O}_3$ -covered Gr. Data is shown for the same samples before (lighter shade) and after (darker shade) of the ALD process. Raman and transport data are taken from different samples at room temperature.

rier density indicates that ALD on  $\text{Ga}_2\text{O}_3$ -covered graphene does not induce additional impurities, in agreement with the Raman spectroscopy results.

Our results demonstrate that liquid-metal synthesized  $\text{Ga}_2\text{O}_3$  is a viable large-area mechanically transferred passivation layer for vdW heterostructures. Encapsulation of graphene by  $\text{Ga}_2\text{O}_3$  preserves the mobility, and reduces ROP scattering in graphene below  $T = 220$  K due to the interplay of high energy phonon modes and dielectric screening in this oxide with intermediate dielectric constant. The large area passivation capability of  $\text{Ga}_2\text{O}_3$  enables other deposition methods without causing damage at the interface, which should allow integration with a variety of materials and processes. The liquid metal printing technique is highly versatile

with a wide range of materials already demonstrated,<sup>19</sup> hence this work opens the possibility of expanding to other liquid metal printed ultrathin materials for large-area vdW heterostructures.

## ACKNOWLEDGEMENTS

This work was supported by the ARC Centre of Excellence in Future Low-Energy Electronics Technologies (CE170100039). We acknowledge Dr. Kaijian Xing for discussions regarding dielectric constant of  $\text{Ga}_2\text{O}_3$  and Mr. Matthias Wurdack for discussions regarding the transfer process of  $\text{Ga}_2\text{O}_3$ .

This work was performed in part at the Melbourne Centre for Nanofabrication (MCN) in the Victorian Node of the Australian National



Fabrication Facility (ANFF).

### III. REFERENCES

- [1] K. S. Novoselov, A. Mishchenko, A. Carvalho, and A. H. Castro Neto, “2D materials and van der Waals heterostructures,” *Science* **353**, aac9439 (2016).
- [2] C. R. Dean, A. F. Young, I. Meric, C. Lee, L. Wang, S. Sorgenfrei, K. Watanabe, T. Taniguchi, P. Kim, K. L. Shepard, and J. Hone, “Boron nitride substrates for high-quality graphene electronics,” *Nat. Nanotechnol.* **5**, 722–726 (2010).
- [3] Alexander S. Mayorov, Roman V. Gorbachev, Sergey V. Morozov, Liam Britnell, Rashid Jalil, Leonid A. Ponomarenko, Peter Blake, Kostya S. Novoselov, Kenji Watanabe, Takashi Taniguchi, and A. K. Geim, “Micrometer-Scale Ballistic Transport in Encapsulated Graphene at Room Temperature,” *Nano Lett.* **11**, 2396–2399 (2011).
- [4] Jiamin Xue, Javier Sanchez-Yamagishi, Danny Bulmash, Philippe Jacquod, Aparna Deshpande, K Watanabe, T Taniguchi, Pablo Jarillo-Herrero, and Brian J LeRoy, “Scanning tunnelling microscopy and spectroscopy of ultra-flat graphene on hexagonal boron nitride,” *Nat. Mater.* **10**, 282–285 (2011).
- [5] Régis Decker, Yang Wang, Victor W Brar, William Regan, Hsin-Zon Tsai, Qiong Wu, William Gannett, Alex Zettl, and Michael F Crommie, “Local electronic properties of graphene on a bn substrate via scanning tunneling microscopy,” *Nano Lett.* **11**, 2291–2295 (2011).
- [6] Ling Lu, Zhiyu Wang, Dexin Ye, Lixin Ran, Liang Fu, John D. Joannopoulos, and Marin Soljačić, “Experimental observation of Weyl points,” *Science* **349**, 622–624 (2015).
- [7] Ali Zavabeti, Azmira Jannat, Li Zhong, Azhar Ali Haidry, Zhengjun Yao, and Jian Zhen Ou, “Two-Dimensional Materials in Large-Areas: Synthesis, Properties and Applications,” *Nano-Micro Lett.* **12**, 66 (2020).
- [8] K. S. Novoselov, V. I. Falko, L. Colombo, P. R. Gellert, M. G. Schwab, and K. Kim, “A roadmap for graphene,” *Nature* **490**, 192–200 (2012).
- [9] Graphene Flagship, “European roadmap for graphene science and technology,” (2019).
- [10] Andrea C. Ferrari, Francesco Bonaccorso, Vladimir Fal’ko, Konstantin S. Novoselov, Stephan Roche, Peter Bøggild, Stefano Borini, Frank H. L. Koppens, Vincenzo Palermo, Nicola Pugno, José A. Garrido, Roman Sordan, Alberto Bianco, Laura Ballerini, Maurizio Prato, Eleftherios Lidorikis, Jani Kivioja, Claudio Marinelli, Tapani Ryhänen, Alberto Morpurgo, Jonathan N. Coleman, Valeria Nicolosi, Luigi Colombo, Albert Fert, Mar Garcia-Hernandez, Adrian Bachtold, Grégory F. Schneider, Francisco Guinea, Cees Dekker, Matteo Barbone, Zhipei Sun, Costas Galiotis, Alexander N. Grigorenko, Gerasimos Konstantatos, Andras Kis, Mikhail Katsnelson, Lieven Vandersypen, Annick Loiseau, Vittorio Morandi, Daniel Neumaier, Emanuele Treossi, Vittorio Pellegrini, Marco Polini, Alessandro Tredicucci, Gareth M. Williams, Byung Hee Hong, Jong-Hyun Ahn, Jong Min Kim, Herbert Zirath, Bart J. van Wees, Herre van der Zant, Luigi Occhipinti, Andrea Di Matteo, Ian A. Kinloch, Thomas Seyller, Etienne Quesnel, Xinliang Feng, Ken Teo, Nalin Rupesinghe, Pertti Hakonen, Simon R. T. Neil, Quentin Tannock, Tomas Löfwander, and Jari Kinaret, “Science and technology roadmap for graphene, related two-dimensional crystals, and hybrid systems,” *Nanoscale* **7**, 4598–4810 (2015).
- [11] J.-H. Chen, C. Jang, S. Adam, M. S. Fuhrer, E. D. Williams, and M. Ishigami, “Charged-impurity scattering in graphene,” *Nat. Phys.* **4**, 377–381 (2008).
- [12] C. Jang, S. Adam, J.-H. Chen, E. D. Williams, S. Das Sarma, and M. S. Fuhrer, “Tuning the Effective Fine Structure Constant in Graphene: Opposing Effects of Dielectric Screening on Short- and Long-Range Potential Scattering,” *Phys. Rev. Lett.* **101**, 146805 (2008).
- [13] S. Fratini and F. Guinea, “Substrate-limited electron dynamics in graphene,” *Phys. Rev. B* **77**, 195415 (2008).
- [14] Jian-Hao Chen, Chaun Jang, Shudong Xiao, Masa Ishigami, and Michael S. Fuhrer, “Intrinsic and extrinsic performance limits of graphene devices on SiO<sub>2</sub>,” *Nat. Nanotechnol.* **3**, 206–209 (2008).
- [15] Aniruddha Konar, Tian Fang, and Debdeep Jena, “Effect of high- $\kappa$  gate dielectrics on charge transport in graphene-based field effect transistors,” *Phys. Rev. B* **82**, 115452 (2010).
- [16] Ali Zavabeti, Jian Zhen Ou, Benjamin J. Carey, Nitu Syed, Rebecca Orrell-Trigg, Edwin L. H. Mayes, Chenglong Xu, Omid Kavehei, Anthony P. O’Mullane, Richard B. Kaner, Kourosh Kalantar-zadeh, and Torben

- Daeneke, “A liquid metal reaction environment for the room-temperature synthesis of atomically thin metal oxides,” *Science* **358**, 332–335 (2017).
- [17] Kourosh Kalantar-zadeh, Jian Zhen Ou, Torben Daeneke, Arnan Mitchell, Takayoshi Sasaki, and Michael S. Fuhrer, “Two dimensional and layered transition metal oxides,” *Applied Materials Today* **5**, 73–89 (2016).
- [18] T. Daeneke, K. Khoshmanesh, N. Mahmood, I. A. de Castro, D. Esrafilzadeh, S. J. Barrow, M. D. Dickey, and K. Kalantar-zadeh, “Liquid metals: fundamentals and applications in chemistry,” *Chem. Soc. Rev.* **47**, 4073–4111 (2018).
- [19] Patjaree Aukarasereenont, Abigail Goff, Chung Kim Nguyen, Chris F. McConville, Aaron Elbourne, Ali Zavabeti, and Torben Daeneke, “Liquid metals: an ideal platform for the synthesis of two-dimensional materials,” *Chem. Soc. Rev.* **51**, 1253 (2022).
- [20] Matthias Wurdack, Tinghe Yun, Eliezer Estrecho, Nitu Syed, Semonti Bhattacharyya, Maciej Pieczarka, Ali Zavabeti, Shao-Yu Chen, Benedikt Haas, Johannes Müller, Mark N. Lockrey, Qiaoliang Bao, Christian Schneider, Yuerui Lu, Michael S. Fuhrer, Andrew G. Truscott, Torben Daeneke, and Elena A. Ostrovskaya, “Ultrathin  $\text{Ga}_2\text{O}_3$  Glass: A Large-Scale Passivation and Protection Material for Monolayer  $\text{WS}_2$ ,” *Adv. Mater.* **33**, 2005732 (2021).
- [21] M. Passlack, N. E. J. Hunt, E. F. Schubert, G. J. Zydzik, M. Hong, J. P. Mannaerts, R. L. Opila, and R. J. Fischer, “Dielectric properties of electron-beam deposited  $\text{Ga}_2\text{O}_3$  films,” *Appl. Phys. Lett.* **64**, 2715–2717 (1994).
- [22] Lei Liao and Xiangfeng Duan, “Graphene-Dielectric Integration for Graphene Transistors,” *Materials Science & Engineering. R, Reports : a review journal* **70**, 354–370 (2010).
- [23] A. K. M. Newaz, Yevgeniy S. Puzyrev, Bin Wang, Sokrates T. Pantelides, and Kirill I. Bolotin, “Probing charge scattering mechanisms in suspended graphene by varying its dielectric environment,” *Nat. Commun.* **3**, 734 (2012).
- [24] Shaffique Adam, E. H. Hwang, V. M. Galitski, and S. Das Sarma, “A self-consistent theory for graphene transport,” *Proc. Natl. Acad. Sci. U. S. A.* **104**, 18392–18397 (2007).
- [25] P Blake, R Yang, SV Morozov, F Schedin, LA Ponomarenko, AA Zhukov, RR Nair, IV Grigorieva, KS Novoselov, and AK Geim, “Influence of metal contacts and charge inhomogeneity on transport properties of graphene near the neutrality point,” *Solid State Commun.* **149**, 1068–1071 (2009).
- [26] K. Zou, X. Hong, D. Keefer, and J. Zhu, “Deposition of High-Quality  $\text{HfO}_2$  on Graphene and the Effect of Remote Oxide Phonon Scattering,” *Phys. Rev. Lett.* **105**, 126601 (2010).
- [27] Massimo V. Fischetti, Deborah A. Neumayer, and Eduard A. Cartier, “Effective electron mobility in Si inversion layers in metal–oxide–semiconductor systems with a high-K insulator: The role of remote phonon scattering,” *J. Appl. Phys.* **90**, 4587–4608 (2001).
- [28] Babak Fallahazad, Seyoung Kim, Luigi Colombo, and Emanuel Tutuc, “Dielectric thickness dependence of carrier mobility in graphene with  $\text{HfO}_2$  top dielectric,” *Appl. Phys. Lett.* **97**, 123105 (2010).
- [29] Xiaohui Tang, Nicolas Reckinger, Olivier Poncelet, Pierre Louette, Ferran Ureña, Hosni Idrissi, Stuart Turner, Damien Cabosart, Jean-François Colomer, Jean-Pierre Raskin, Benoit Hackens, and Laurent A. Francis, “Damage evaluation in graphene underlying atomic layer deposition dielectrics,” *Sci. Rep.* **5**, 13523 (2015).
- [30] Zhi Jin, Yongbo Su, Jianwu Chen, Xinyu Liu, and Dexin Wu, “Study of  $\text{AlN}$  dielectric film on graphene by Raman microscopy,” *Appl. Phys. Lett.* **95**, 233110 (2009).
- [31] B. Dlubak, P. Seneor, A. Anane, C. Barraud, C. Deranlot, D. Deneuve, B. Servet, R. Mattana, F. Petroff, and A. Fert, “Are  $\text{Al}_2\text{O}_3$  and  $\text{MgO}$  tunnel barriers suitable for spin injection in graphene?” *Appl. Phys. Lett.* **97**, 092502 (2010).
- [32] Mohammad H. Maneshian, Fang-Ling Kuo, Kristopher Mahdak, Junyeon Hwang, Rajarshi Banerjee, and Nigel D. Shepherd, “The influence of high dielectric constant aluminum oxide sputter deposition on the structure and properties of multilayer epitaxial graphene,” *Nanotechnology* **22**, 205703 (2011).